JOURNAL OF GEOPHYSICAL RESEARCH, VOL. 112, D10120, doi:10.1029/2006JD007683, 2007

An analysis of the regulation of tropical tropospheric water vapor

A. E. Dessler[1] and K. Minschwaner[2]

Received 21 June 2006; revised 24 January 2007; accepted 28 January 2007; published 26 May 2007.

[1] We use a simple trajectory model to investigate the mechanisms that regulate mid- and upper-tropospheric humidity. Our model advects water passively and contains no microphysics other than the requirement that water vapor is immediately removed so as to prevent the relative humidity from ever exceeding 100%. We demonstrate that our model accurately reproduces H_2O measurements made by the Atmospheric Infrared Sounder onboard NASA's Aqua satellite. Our results show that, given the large-scale circulation of the troposphere, detailed microphysics need not be included in order to accurately simulate H_2O. We have also identified three preferred regions where air parcels in the mid and upper troposphere experience their final dehydration. The first is in the equatorial upper troposphere and is associated with convective outflow at the top of the tropical Hadley circulation. Final dehydration of air that detrains at potential temperature θ above $\sim$340 K ($\sim$10 km) predominantly occurs here. The other two regions are found at lower altitudes in the midlatitudes of both hemispheres and are associated with dehydration during isentropic excursions to midlatitudes. Final dehydration of air that detrains at θ below $\sim$340 K predominantly occurs here. Finally, we analyze the water budget of the dry eastern Pacific subtropics and find that dehydration in both the equatorial upper troposphere and the midlatitudes contribute to the dryness there.

Citation: Dessler, A. E., and K. Minschwaner (2007), An analysis of the regulation of tropical tropospheric water vapor, *J. Geophys. Res.*, *112*, D10120, doi:10.1029/2006JD007683.

1. Introduction

[2] Water vapor is the most important greenhouse gas in the atmosphere. As such, understanding the mechanisms that regulate it is of central importance for understanding past and future climate change. It is often argued that microphysical processes occurring in and around convection play a key role in regulating tropospheric humidity [e.g., *Rennó et al.*, 1994; *Emanuel and Pierrehumbert*, 1995; *Emanuel and Zivkovic-Rothman*, 1999; *Lindzen et al.*, 2001]. This would suggest that detailed microphysics must be included in climate models in order for them to accurately simulate tropospheric humidity. Present-day climate models do not include detailed microphysics, and the prospects of adding them in the near future appear dim owing to their high computational expense. Thus if detailed microphysics are indeed necessary for accurate predictions of our climate, then predictions of future warming made by today's climate models must be viewed as highly uncertain.

[3] Over the past 10 years, however, an alternative school of thought has emerged: that detailed microphysics need not be included in models in order to accurately simulate tropical tropospheric humidity. The view is based on results of simplified models of the troposphere that advect water passively and contain virtually no microphysics other than the requirement that water vapor is immediately removed so as to prevent the relative humidity (RH) from exceeding 100%. These simple models are sometimes referred to as large-scale control (LSC) models, and, despite their simplicity, they have proven effective in simulating tropical upper tropospheric humidity [*Sherwood*, 1996; *Salathe and Hartmann*, 1997, 2000; *Pierrehumbert and Roca*, 1998; *Dessler and Sherwood*, 2000; *Folkins et al.*, 2002b; *Minschwaner and Dessler*, 2004].

[4] Previous analyses of LSC-based models have compared model reconstructions of tropospheric H_2O to relatively crude measurements of H_2O in the mid and upper troposphere. In this paper, we will compare reconstructions of tropospheric H_2O from our trajectory-based LSC model to measurements of H_2O from the Atmospheric Infrared Sounder (AIRS) onboard NASA's Aqua satellite. The AIRS data set provides high vertical resolution and high-accuracy measurements, as well as the ability to retrieve H_2O in partially cloudy regions. It is therefore an improvement over previous tropospheric H_2O measurements and provides a high-quality data set to test the LSC model against. We will also analyze our model in order to determine what mechanisms are most important in regulating tropospheric humidity, following along the same lines as the recent paper by *Galewsky et al.* [2005].

[5] In section 2, we describe the AIRS measurements and the trajectory-based LSC model. In section 3, we compare the model's H_2O simulations to AIRS measurements in the

[1]Department of Atmospheric Sciences, Texas A&M University, College Station, Texas, USA.
[2]Department of Physics, New Mexico Institute of Mining and Technology, Socorro, New Mexico, USA.

0148-0227/07/2006JD007683$09.00

mid and upper troposphere. In section 4, we analyze the model to gain insight into the mechanisms that regulate mid- and upper-tropospheric humidity. In section 5, we present our conclusions.

2. Data and Model

2.1. AIRS Measurements

[6] AIRS measurements of H_2O vapor mixing ratio (in g/kg) were obtained from 1 March 2003 through 28 February 2004 and nearly cover the tropics each day, with equator crossing times of 1:30 am and 1:30 pm local solar time. Throughout the rest of the paper, references to "H_2O" refer to the vapor phase exclusively; references to condensate will be explicitly noted. The horizontal resolution of the AIRS footprint is ~14 km (nadir), but retrievals are done on a three-by-three matrix of AIRS footprints, meaning that the resolution of a single retrieval is ~50 km. Individual AIRS retrievals have a vertical resolution of 2 km and an accuracy of ~10% throughout most of the troposphere [*Fetzer et al.*, 2005, Table 8]. We also note that the AIRS retrieval algorithm incorporates a unique cloud-clearing algorithm [*Susskind et al.*, 2003] that allows retrievals to be made in the presence of up to 80% cloud cover.

[7] In this analysis, we use version 4 of the AIRS' daily level-3 product, in which individual retrievals of H_2O from a single day have been aggregated into $1^\circ \times 1^\circ$ boxes covering the globe. We average the H_2O measurements from the ascending and descending orbits to produce a single value each day in each $1^\circ \times 1^\circ$ box. If there are no data from an ascending or descending orbit, we set the daily average equal to the data from the other orbit. If both orbits are missing, then that grid point is flagged as invalid for that day.

[8] AIRS measurements of H_2O are not retrieved on the AIRS standard pressure levels, but at pressures equal to the geometric mean of adjacent standard levels. In this paper, we will analyze measurements at ~547 hPa (between the 600- and 500-hPa standard levels) and ~346 hPa (between the 400- and 300-hPa standard levels), corresponding to altitudes of around 5 and 9 km, respectively. We focus on these levels because changes in H_2O here have the strongest impact on radiative forcing of the surface-troposphere system [e.g., *Held and Soden*, 2000].

2.2. Trajectory Simulations

[9] We will compare the AIRS measurements to simulations of H_2O at 547 and 346 hPa from a trajectory-based LSC model. To determine the H_2O at a given location X_o and time t_o, we begin by running a trajectory from that location and time backwards for 30 days. The trajectories use horizontal and vertical winds from the 6-hourly NCEP reanalysis [*Kalnay et al.*, 1996] and are numerically integrated with a fourth-order Runge-Kutta scheme using a fixed time step of 1/100 of a day. We use here the same integrator as was used by *Dessler and Sherwood* [2000].

[10] We determine the H_2O at X_o and t_o using the following method. First, we examine the back trajectory in order to determine the last time the parcel encountered convection. We consider a parcel as "encountering convection" whenever the parcel's potential temperature (θ) increases by more than a prescribed threshold value (without regard for how long it takes for the θ increase to occur). This approach is adopted because the dominant process increasing θ in the troposphere is convection.

[11] We assume that the RH of the parcel is set to 100% by its encounter with convection (all RH values in this paper are with respect to ice). After the convective encounter, H_2O is advected passively along the trajectory except when temperature decreases enough to lead to RH > 100%. When that happens, excess H_2O is removed so as to keep the RH equal to 100%. In other words, the H_2O at the end of the trajectory is equal to the minimum saturation H_2O that occurred along the trajectory after the most recent encounter with convection.

[12] To simulate the tropical H_2O field for a given day, we follow this procedure for a grid of points matching the AIRS level-3 grid (1° latitude $\times$ 1° longitude) from 30°N to 30°S, and at 547 and 346 hPa. All trajectory integrations begin at 1200 UT. This approach is similar to the reverse-domain filling procedure of *Sutton et al.* [1994], which is widely used for reconstructing constituent fields. We simulate daily H_2O this way for every day from 1 March 2003 through 28 February 2004.

[13] An adjustable parameter in our model is the threshold used to identify encounters with convection. Our "standard model" uses a threshold of $1/3(\theta_{max} - 300)$, where θ_{max} is the maximum θ (in K) that the parcel experiences over its 30-day trajectory. Thus if a particular parcel reaches a maximum θ of 375 K, then the convective threshold is 25 K. Anytime this particular parcel's θ increases by 25 K, we consider it to have encountered convection. This threshold is arbitrary, but reasonable based on a manual review of a hundred or so trajectories. To evaluate our sensitivity to this arbitrary choice, we have also tested two other thresholds in this analysis. One is a fixed 10-K threshold, while the other uses a threshold of $1/2(\theta_{max} - 300)$. We will discuss the sensitivity to this threshold in the next section.

[14] About one quarter of the parcels never experience an increase in θ greater than the convective threshold; these parcels are considered indeterminate and are excluded from any analyses. Of those that do encounter convection, most experience it within the last few days of the trajectory. For parcels initialized at 547 hPa, for example, 80% have experienced convection within the previous 2 days, 91% within 5 days, and 97% in 10 days.

[15] This LSC model is similar to one that has been used previously in successful investigations of tropospheric humidity by *Dessler and Sherwood* [2000] and *Waugh* [2005], although there are some differences. In particular, we adopt here a new initialization scheme that we believe is more physically reasonable.

3. Model Simulations and Comparisons to Data

3.1. The LSC Model Versus AIRS

[16] Figure 1 shows average H_2O between 1 March 2003 and 28 February 2004, calculated by the trajectory model. At both 346 and 547 hPa, regions of high H_2O are found over South America, equatorial Africa, and the western Pacific, all regions of intense convection. One can also see the intertropical convergence zone and the southern Pacific convergence zone clearly reflected in the H_2O field.

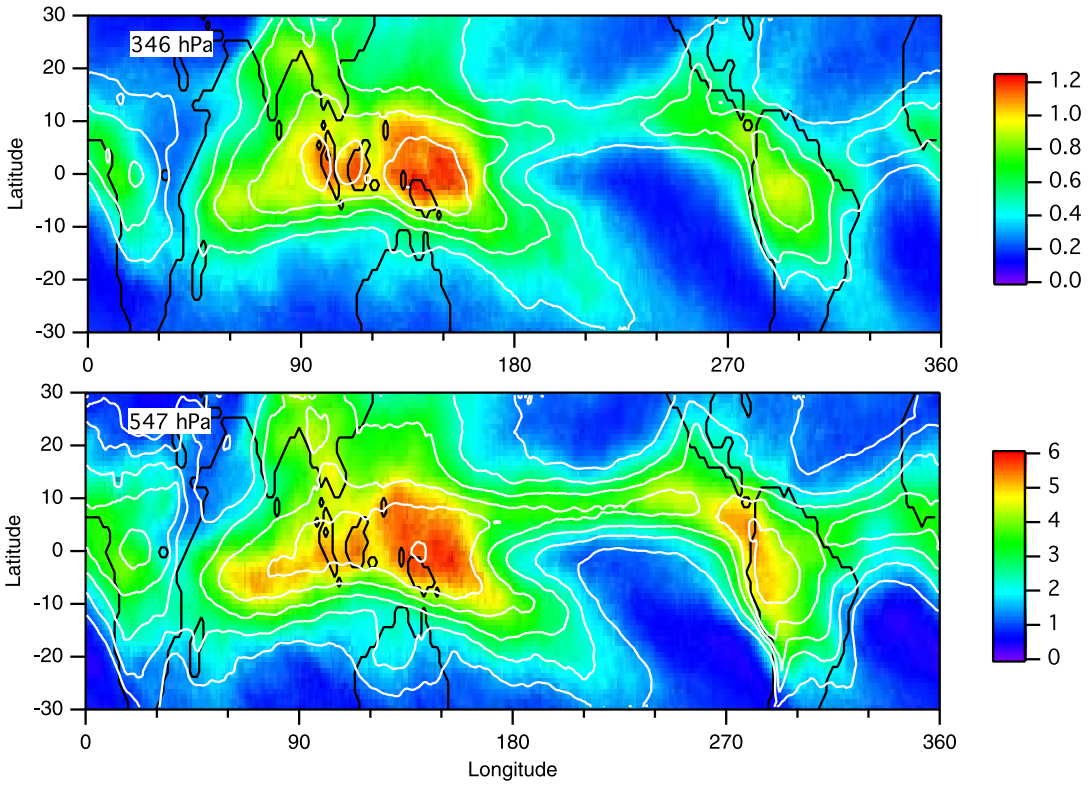

Figure 1. Model-simulated H_2O mixing ratio (g/kg) at 346 hPa (top) and 547 hPa (bottom), averaged from 1 March 2003 to 28 Feb. 2004. White contours are contours of AIRS-measured H_2O in the 400- to 300-hPa layer (top) and the 600- to 500-hPa layer (bottom). In the top plot, the outer contour is 0.4 g/kg and the interval is 0.15 g/kg; in the bottom plot, the outer contour is 1.5 g/kg and the interval is 0.625 g/kg.

[17] Overlying the model are contours of AIRS H_2O measurements, averaged over the same period. To avoid sampling biases, the average at each grid point contains only those days with both a valid AIRS measurement and a valid H_2O trajectory value at that grid point. As a result, the set of days going into the grid-point average may vary from point to point. Figure 1 plainly shows that the AIRS contours closely mimic the model-simulated distribution of H_2O. We conclude that the trajectory model accurately reproduces the horizontal gradients of H_2O at both 346 and 547 hPa.

[18] The frequency of occurrence of the annual-average H_2O values plotted in Figure 1 is shown as histograms in Figure 2. This figure shows three model simulations at each altitude, each using a different convective threshold (see section 2.2). The differences between these models are small, showing that the model results are robust with respect to this parameter. Overall, the ensemble of trajectory models reproduces the observed H_2O values accurately, particularly at 346 hPa. At 547 hPa, the model overpredicts the occurrence of the highest and lowest H_2O values. This might be due to biases in the data or errors in the model simulations, such as a lack of mixing in the model. *Pierrehumbert and Roca* [1998] also found that their LSC model also overpredicted H_2O in moist regions.

[19] At 547 hPa, the three trajectory-model runs predict a 30°N–30°S average H_2O of 2.21, 2.51, and 2.38 g/kg, compared to the corresponding AIRS average of 2.25, 2.36, and 2.31 g/kg (the AIRS average also varies between the model runs because the number of trajectories that encounter convection varies between runs, and only AIRS values

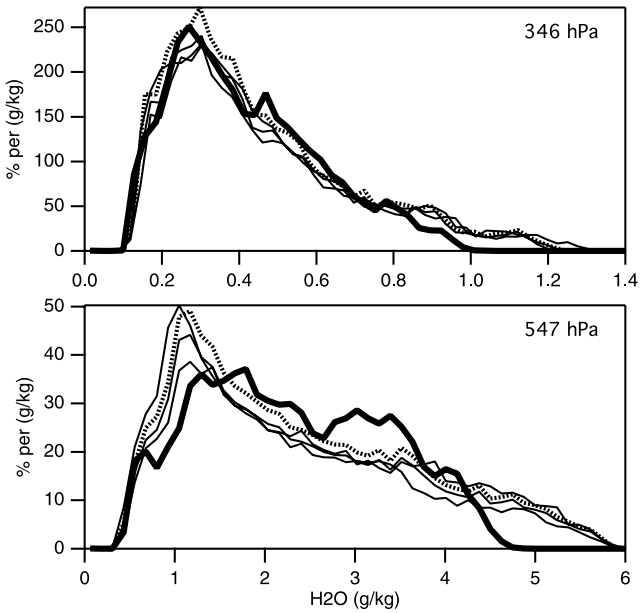

Figure 2. Histograms of annual average H_2O mixing ratio (g/kg) at 346 hPa (top) and 547 hPa (bottom). The thick solid lines are histograms of the AIRS data from Figure 1. The three thin solid lines are histograms from the trajectory model, each using a different convective threshold. The dotted line is obtained using the standard trajectory model with a RH limit of 90%.

corresponding to trajectories encountering convection are included in the average). At 346 hPa, the model runs have average values of 0.45, 0.46, and 0.45 g/kg, and AIRS has average values of 0.41, 0.43, and 0.42 g/kg. Thus the LSC model tends to predict higher H_2O than measured by AIRS, although the differences are all within the uncertainty of the AIRS H_2O measurements.

[20] Besides the convective threshold, the other free parameter in the model is the 100% RH threshold. When considering large spatial scales, such as the $1^\circ \times 1^\circ$ grid that the AIRS data are averaged over, it is possible for saturation and subsequent removal of H_2O to be occurring over a small fraction of this area even when the area-averaged RH is below 100%. To account for these subgrid-scale processes, *Galewsky et al.* [2005] and *Sherwood* [1996] both assumed that saturation and removal occurred in their models when the grid-averaged RH exceeded 90%. Figure 2 also shows the distribution from the standard model when RH_{max} was set at 90% rather than 100%. Average H_2O at 547 and 346 hPa is reduced by 10% below the values predicted using RH_{max} of 100%. This does not materially improve agreement between the model and data, so in the rest of the paper, we will use RH_{max} of 100%. We recognize, however, that this remains an uncertainty in our analysis and deserving of additional research.

[21] There are potential errors in the trajectory model, including missing microphysics, errors in the wind fields, and unresolved small-scale motions in the wind fields. These are discussed in the work of *Dessler and Sherwood* [2000], and we will not repeat them here. The upshot is that, while uncertainties exist, there is abundant evidence in this paper and in previous analyses that LSC models accurately simulate the observed mid- and upper-troposphere H_2O abundance.

3.2. Implications of the Comparison

[22] The good agreement between the AIRS data and our LSC model in the mid and upper troposphere is consistent with previous trajectory-based LSC studies [e.g., *Salathe and Hartmann*, 1997, 2000; *Pierrehumbert*, 1998; *Pierrehumbert and Roca*, 1998; *Dessler and Sherwood*, 2000]. However, most previous LSC models have been compared to H_2O measurements from nadir-viewing infrared radiometers. These infer H_2O averaged over a layer $\sim$6 km thick and are only able to make measurements in clear skies [e.g., *Soden and Bretherton*, 1996]. The AIRS data are a substantial improvement over those data sets.

[23] As a result, the good agreement shown in this paper strengthens the conclusion that, given the large-scale wind field, mid- and upper-tropospheric H_2O can be predicted by a model that contains the simple microphysical assumption of a fixed RH limit of 100%. In other words, detailed microphysics are not required in the H_2O vapor continuity equation in order to accurately simulate the H_2O budget.

[24] This does not acquit microphysics entirely of playing a role in regulating tropospheric H_2O. It is possible that microphysical processes determine in part the large-scale wind field. If so, then microphysical processes might still be important in determining the H_2O budget. Our work is agnostic on this question. However, we note that that is not what is asserted by those arguing for microphysical control of H_2O. *Lindzen et al.* [2001], for example, claim that microphysics regulate the amount of H_2O ice detraining from convection, and that this ice serves as an important moisture source for the troposphere. Our work provides no support for that argument.

[25] We have also directly tested the importance of H_2O ice transport with a version of our standard model that includes delayed sedimentation of ice. In this model, ice is not removed immediately, but with a timescale of 1 day. This is similar to what was done by *Dessler and Sherwood* [2000] to test ice transport in the upper troposphere. At 346 and 547 hPa, the average H_2O in the delayed-sedimentation model is 1.4 and 6.3 g/kg. These values are much higher than either AIRS measurements or the instantaneous sedimentation models, clearly showing the hydrating power of transported ice.

[26] Obviously, adding any nonzero sedimentation time will necessarily increase the model-predicted H_2O. Since the model with instantaneous sedimentation generally overestimates the AIRS measurements already, adding a finite ice lifetime will automatically degrade the agreement between the data and model. Thus in agreement with *Dessler and Sherwood* [2000], we conclude that we see no evidence that transport and evaporation of ice is an important source of H_2O in the troposphere.

4. Dehydration in the Model

[27] In our trajectory-based LSC model, the H_2O abundance at the end of a trajectory is equal to the minimum saturation H_2O that occurs after the most recent encounter with convection. We can therefore identify the location of the minimum saturation H_2O (also referred to as location of "final dehydration"), and in this section, we analyze those locations.

[28] Figure 3a plots the probability distribution of the latitude of final dehydration as a function of the detrainment θ for parcels initialized at 547 hPa ($\sim$322-K θ) (detrainment θ is defined as the highest θ obtained during or after the last encounter with convection). We note that the detrainment θ is a good approximation of the final dehydration θ. At both 547 and 346 hPa, about 90% of the parcels experience their final dehydration within 4 K of the detrainment θ.

[29] Figure 3a shows several maxima in the probability distribution. One maximum is centered roughly over the equator at $\sim$345-K θ. This maximum is collocated with a maximum in convective detrainment mass flux [e.g., *Folkins et al.*, 2002a] associated with outflow at the top of the tropical Hadley circulation. These parcels experience dehydration during the rapid cooling that occurs during upward transport in deep convective events. For parcels that detrain above 345 K and are dehydrated between 15°N and 15°S (70% of all parcels detraining above 345 K), we find that 52% detrain fully dehydrated from convection. For the other 48%, isentropic cooling events occurring 1 to 2 days after detrainment lead to saturation, further loss of water, and final dehydration. We will refer to this dehydration maximum as "deep-tropical dehydration."

[30] Two other maxima in Figure 3a are located at 30°–40° in each hemisphere and centered at $\sim$335 K. In fact, 57% of all parcels detraining below 345 K achieve final dehydration poleward of 25° compared to just 13% for parcels detraining above 345 K. To understand why, we plot

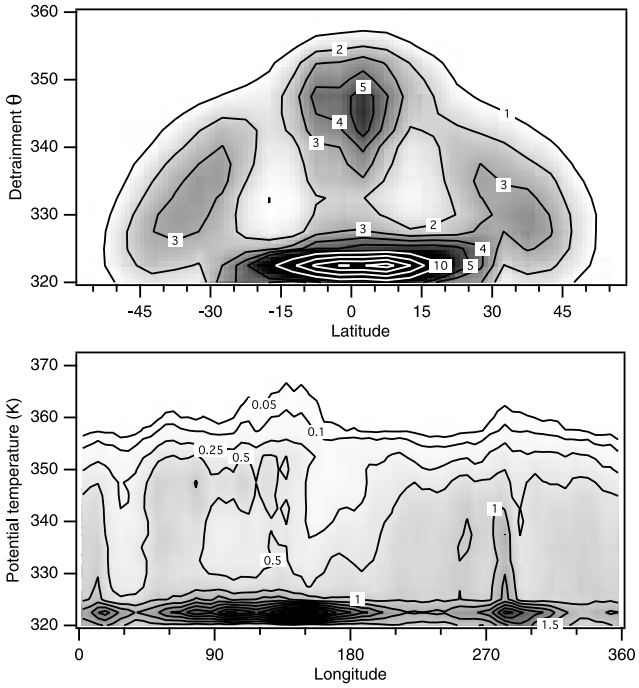

Figure 3. Two-dimensional probability distribution (in 10^{-2}%) of dehydration location versus detrainment θ, based on the set of trajectories initialized at 547 hPa (~322-K θ). The top plot is versus latitude; the bottom plot is versus longitude. The figures are shaded to improve readability. In the top plot, white contours have values greater than 10, and their contour interval is 5.

in Figure 4 annual- and zonal-averaged contours of θ. Below ~345 K, isentropes slope upward with increasing latitude. Air mixing isentropically into midlatitudes will experience ascent and cooling associated with the upward tilt of these isentropes. In our model, this leads to condensation and loss of water; when the air returns to tropical latitudes, it is drier than when it left. *Kelly et al.* [1991] invoked a similar mechanism to explain the asymmetry of upper tropospheric water between the northern and southern midlatitudes, and *Galewsky et al.* [2005] also identified this mechanism in their analyses of the subtropical humidity budget. We will refer to this process as "midlatitude dehydration."

[31] We also note that θ surfaces above 345 K slope downward with increasing latitude, so mixing into the midlatitudes at these altitudes will result in descent and warming, and no dehydration. This explains why parcels detraining above 345 K tend not to experience midlatitude dehydration.

[32] Dehydration occurs infrequently at all altitudes in the subtropics (15°–25° in both hemispheres). There is little convection at these latitudes, so dehydration during diabatic ascent is rare. Also, the isentropes are generally horizontal over this latitude range, so there is also little cooling and dehydration associated with mixing on the isentropes.

[33] There is also a maximum at 325 K between 15° N and 15° S. 325 K is approximately 547 hPa, so this maximum corresponds to parcels that are still ascending in convection and have not yet experienced their final dehydration. It also includes some parcels that defrained recently right at 547 hPa.

[34] The pattern of final dehydration for parcels initialized at 346 hPa (not shown) is quite similar to those at 547 hPa. For parcels detraining above 345 K (about two thirds of the parcels), deep-tropical dehydration dominates. Midlatitude dehydration dominates for parcels detraining below 345 K.

[35] Figure 3b shows the longitude distribution of the location of final dehydration. Final dehydration occurs at most longitudes, but with definite minima in dehydration frequency around longitudes of 30° and 150°–180°.

[36] To complete the picture, Figure 5 shows the latitude and longitude distribution of the final dehydration locations of parcels that detrain at 345 and 335 K. Figure 5a shows that parcels that detrain at 345-K θ are primarily dehydrated in the deep tropics, consistent with Figure 3a.

[37] Figure 5b shows that parcels that detrain at 335-K θ are preferentially dehydrated in the midlatitudes and at longitudes between 180° and 360°. There is also significant dehydration occurring off the West Coast of equatorial South America and Africa. These parcels come from midlevel detrainment from intense continental convection. Perhaps surprisingly, dehydration in the western Pacific is largely absent for 335-K detrainment.

[38] Figures 6a and 6b show the time series of the latitude of dehydration of parcels that detrain at 350 and 335 K, respectively. Figure 6a shows that parcels that detrain at 350 K are dehydrated primarily in the deep tropics, and that significant seasonal variations are apparent. In Northern Hemisphere (NH) winter, dehydration occurs in primarily north of the equator, between 0° and 10°N. Six months later, in Southern Hemisphere winter, dehydration occurs south of the equator, between 0° and 10°S. During spring and fall, dehydration is more evenly spread across the tropics.

[39] Figure 6b shows the time series for air that detrains at 335-K θ. One can again see a clear seasonal cycle in the midlatitude dehydration, with this dehydration tending to occur in the winter hemisphere, lasting into early spring. The equatorial dehydration at this level occurs predominantly during NH summer and winter, with less occurring during NH spring and fall.

[40] Finally, one can infer from Figure 1 that the convection predominantly hydrates its local environment [e.g., *Udelhofen and Hartmann*, 1995]. In Figure 7, we quantify

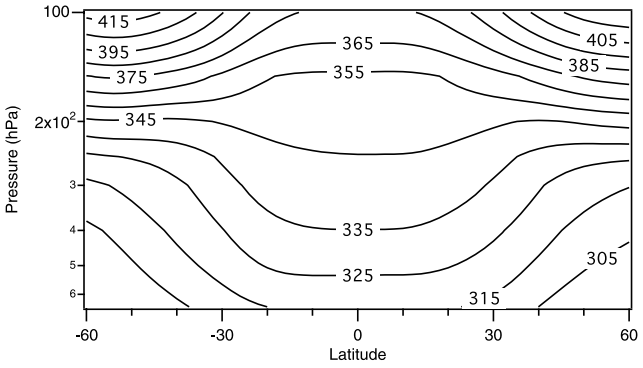

Figure 4. Contours of zonally averaged θ surfaces from NCEP reanalysis, averaged over the period from 1 March 2003 to 28 February 2004.

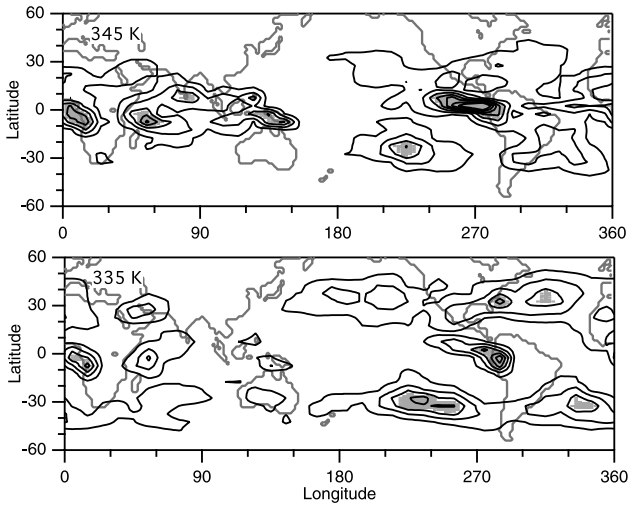

Figure 5. Latitude and longitude distribution of parcel dehydration. (a) Horizontal distribution of dehydration for parcels that detrain at 345 ± 2-K θ; (b) same quantity for those parcels detraining at 335 ± 2-K θ. The quantity plotted is % per degree of longitude per degree of latitude. In both plots, the contours are 3, 6, 9, ... $\times 10^{-3}$ %, and regions with values >10 $\times 10^{-3}$ % are shaded.

this by plotting a two-dimensional probability distribution of H_2O and distance from convective detrainment for the trajectories for an evenly distributed subset of grid points from Figure 1.

[41] Figure 7 shows that a parcel contains relatively high values of H_2O only if it is near where it detrained. At 346 hPa, one third of the parcels have >0.5 g/kg of H_2O, and 90% of those parcels are found within 2000 km of their

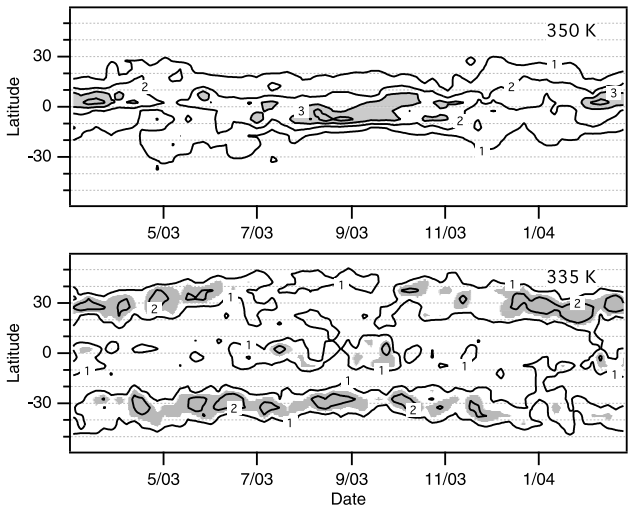

Figure 6. Time series of the latitude of dehydration of parcels that detrain at (a) 350 ± 2-K θ and (b) 335 ± 2-K θ. The units are % per degree of latitude; integral over all latitudes on any given day yields 100%. In both plots, the contour interval is 1%. In the top and bottom plots, fractions > 3% and 1.5% are shaded, respectively.

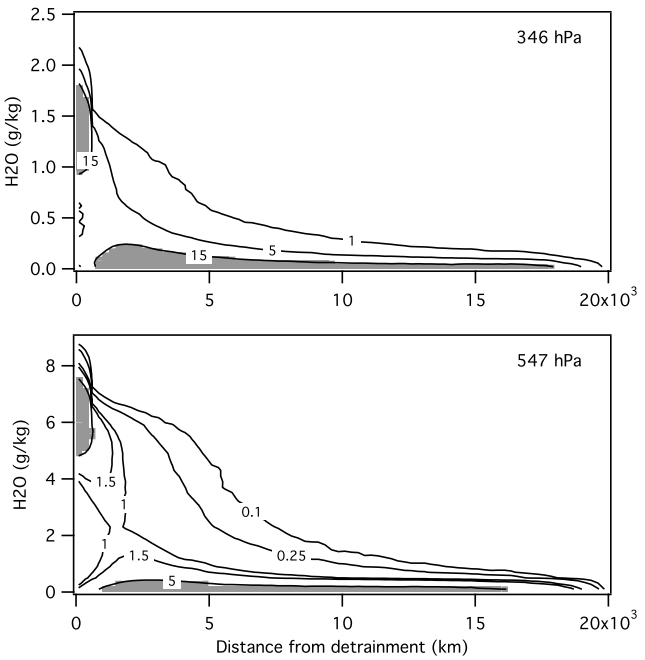

Figure 7. Two-dimensional probability distribution of H_2O abundance at the end of the trajectory and distance from detrainment from convection. Parcels are initialized at (top) 346 hPa and (bottom) 547 hPa. Units are 10^{-3} %, and regions with frequency > 15 $\times 10^{-3}$ and 5 $\times 10^{-3}$ and are shaded in the top and bottom plots, respectively. Integration over the entire domain yields 100%. Distance here is the straight-line distance between the detrainment point and the final location; the actual distance the trajectory followed between these points might be considerably greater.

detrainment location. At 547 hPa, one third of the parcels have >3.5 g/kg of H_2O, and 90% of those parcels are found within 1300 km of convection. Parcels that originate at greater distances have spent more time in transit and therefore have descended so that their H_2O abundance is small relative to those parcels that have more recently detrained.

[42] The subtropics are far from convection, and, unsurprisingly, one finds low values of H_2O there. *Galewsky et al.* [2005] attribute the dryness of the subtropics primarily to midlatitude dehydration. To investigate this, we analyze the water budget for a very dry subtropical region located at 247.5°–262.5° longitude, 10°S–20°S latitude. At 547 hPa, 34% of the parcels in this dry region detrained above 340 K and were dehydrated between 20°N and 20°S, corresponding to deep-tropical dehydration. These parcels contain an average H_2O value of 0.23 g/kg. Forty-one percent of the parcels were dehydrated poleward of 25°S, corresponding to midlatitude dehydration. These parcels contain an average H_2O value of 0.45 g/kg.

[43] We find a similar result for this same region at 346 hPa. Sixty-one percent of the parcels initialized in this box detrained above 340 K and achieved final dehydration between 20°N and 20°S. Twenty-three percent of the parcels achieved final dehydration poleward of 25°. The average H_2O content of parcels following these two

pathways contained on average about the same H_2O: $\sim$0.13–0.15 g/kg. Thus in contrast to the results of Galewsky et al., we see both deep-tropical and midlatitude dehydration playing important roles in determining the humidity in the subtropics.

5. Conclusions

[44] In this paper, we have used a simple model of mid- and upper-tropospheric H_2O to investigate the mechanisms that regulate tropospheric humidity. In our model, H_2O is advected passively by the atmospheric large-scale circulation, except when the relative humidity (RH, with respect to ice) exceeds 100%. When that happens, H_2O is instantly removed in order to limit the RH to 100%. Comparisons between the model simulations of H_2O and AIRS measurements of H_2O show that the model accurately reproduces the H_2O distribution at 346 and 547 hPa, levels where changes in H_2O have the strongest impact on radiative forcing of the surface-troposphere system [e.g., *Held and Soden*, 2000].

[45] The good agreement between the LSC model and the measurements allows us to strengthen the conclusion reached by previous analyses [*Sherwood*, 1996; *Salathe and Hartmann*, 1997, 2000; *Pierrehumbert and Roca*, 1998; *Dessler and Sherwood*, 2000; *Folkins et al.*, 2002b; *Minschwaner and Dessler*, 2004] that, given the large-scale circulation, it is not necessary to include detailed microphysical processes in a model in order to simulate mid- and upper-tropospheric H_2O. The superiority of the AIRS data set over those used in previous papers means that our analysis provides a particularly strong verification of this conclusion.

[46] This result does not, however, completely eliminate the possibility that inclusion of detailed microphysics is necessary for an accurate simulation of tropospheric H_2O. If detailed microphysical processes play a role in determining the large-scale wind field, then microphysics might indeed be playing an important role in regulating H_2O. Our analysis provides no insight into this question.

[47] Analysis of the model also yields insight into the mechanisms that regulate mid- and upper-tropospheric H_2O. We have identified three dominant regions where final dehydration of mid- and upper-tropospheric air takes place. The first region, over the deep tropics (15°N–15°S) and centered at 345-K potential temperature, is associated with outflow at the top of the tropical Hadley circulation. The other two regions are located in the midlatitudes, and final dehydration of air detraining below $\sim$340 K generally takes place there. Dehydration occurs here because isentropes below 345 K slope upward as one goes poleward, so isentropic mixing into the midlatitudes lead to cooling and dehydration. When the parcels return to the tropics, they are drier than before the excursion. For the dry eastern Pacific, we find that both deep-tropical and midlatitude dehydration play important roles in regulating its humidity.

[48] **Acknowledgments.** We thank R. Saravanan and D. Waugh for helpful comments. This work was supported by a NASA EOS/IDS grant to Texas A&M and by a NASA Aqua, Terra, ACRIM data analysis grant to Texas A&M and to New Mexico Tech.

References

Dessler, A. E., and S. C. Sherwood (2000), Simulations of tropical upper tropospheric humidity, *J. Geophys. Res.*, *105*, 20,155–20,163.

Emanuel, K. A., and R. T. Pierrehumbert (1995), Microphysical and dynamical control of tropospheric water vapor, in *Clouds, Chemistry, and Climate*, edited by P. J. Crutzen and V. Ramanathan, pp. 17–28, Springer, New York.

Emanuel, K. A., and M. Zivkovic-Rothman (1999), Development and evaluation of a convection scheme for use in climate models, *J. Atmos. Sci.*, *56*, 1766–1782.

Fetzer, E. J., A. Eldering, E. F. Fishbein, T. Hearty, W. F. Irion, and B. Kahn (2005), Validation of AIRS/AMSU/HSB core products for data release version 4.0, March 8, 2005, JPL D-31448, 60 pages.

Folkins, I., C. Braun, A. M. Thompson, and J. Witte (2002a), Tropical ozone as an indicator of deep convection, *J. Geophys. Res.*, *107*(D13), 4184, doi:10.1029/2001JD001178.

Folkins, I., K. K. Kelly, and E. M. Weinstock (2002b), A simple explanation for the 11 to 15 km increase in tropical relative humidity, *J. Geophys. Res.*, *107*(D23), 4736, doi:10.1029/2002JD002185.

Galewsky, J., A. Sobel, and I. Held (2005), Diagnosis of subtropical humidity dynamics using tracers of last saturation, *J. Atmos. Sci.*, *62*, 3353–3367.

Held, I. M., and B. J. Soden (2000), Water vapor feedback and global warming, *Annu. Rev. Energy Environ.*, *25*, 441–475.

Kalnay, E., et al. (1996), The NCEP/NCAR 40-year reanalysis project, *Bull. Am. Meteorol. Soc.*, *77*, 437–471.

Kelly, K. K., A. F. Tuck, and T. Davies (1991), Wintertime asymmetry of upper tropospheric water between the Northern and Southern Hemispheres, *Nature*, *353*, 244–247.

Lindzen, R. S., M.-D. Chou, and A. Y. Hou (2001), Does the Earth have an adaptive iris?, *Bull. Am. Meteorol. Soc.*, *82*, 417–432.

Minschwaner, K., and A. E. Dessler (2004), Water vapor feedback in the tropical upper troposphere: Model results and observations, *J. Clim.*, *17*, 1272–1282.

Pierrehumbert, R. T. (1998), Lateral mixing as a source of subtropical water vapor, *Geophys. Res. Lett.*, *25*, 151–154.

Pierrehumbert, R. T., and R. Roca (1998), Evidence for control of Atlantic subtropical humidity by large scale advection, *Geophys. Res. Lett.*, *25*, 4537–4540.

Rennó, N. O., K. A. Emanuel, and P. H. Stone (1994), Radiative-convective model with an explicit hydrologic cycle. 1. Formulation and sensitivity to model parameters, *J. Geophys. Res.*, *99*, 14,429–14,441.

Salathe, E. P., and D. L. Hartmann (1997), A trajectory analysis of tropical upper-tropospheric moisture and convection, *J. Clim.*, *10*, 2533–2547.

Salathe, E. P., and D. L. Hartmann (2000), Subsidence and upper-tropospheric drying along trajectories in a general circulation model, *J. Climate*, *13*, 257–263.

Sherwood, S. C. (1996), Maintenance of the free-tropospheric tropical water vapor distribution. Part II: Simulation by large-scale advection, *J. Clim.*, *9*, 2919–2934.

Soden, B. J., and F. P. Bretherton (1996), Interpretation of TOVS water vapor radiances in terms of layer-average relative humidities: Method and climatology for the upper, middle, and lower troposphere, *J. Geophys. Res.*, *101*, 9333–9343.

Susskind, J., C. D. Barnet, and J. M. Blaisdell (2003), Retrieval of atmospheric and surface parameters from AIRS/AMSU/HSB data in the presence of clouds, *IEEE Trans. Geosci. Remote*, *41*, 390–409.

Sutton, R. T., H. Maclean, R. Swinbank, A. O'Neill, and F. W. Taylor (1994), High-resolution stratospheric tracer fields estimated from satellite observations using Lagrangian trajectory calculations, *J. Atmos. Sci.*, *51*, 2995–3005.

Udelhofen, P. M., and D. L. Hartmann (1995), Influence of tropical cloud systems on the relative humidity in the upper troposphere, *J. Geophys. Res.*, *100*, 7423–7440.

Waugh, D. W. (2005), Impact of potential vorticity intrusions on subtropical upper tropospheric humidity, *J. Geophys. Res.*, *110*, D11305, doi:10.1029/2004JD005664.

A. E. Dessler, Department of Atmospheric Sciences, Texas A&M University, TAMU 3150, College Station, TX 77843, USA. (dessler@ariel.met.tamu.edu)

K. Minschwaner, Department of Physics, New Mexico Institute of Mining and Technology, Socorro NM, USA.